Sains Malaysiana 55(3)(2026): 517-529
http://doi.org/10.17576/jsm-2026-5503-13

Bifurcation Analysis and Chaos Control in a Discrete Fractional- Order Model of Immune Response to Abnormal Cells

(Analisis Bifurkasi dan Kawalan Kekacauan dalam Model Tertib Pecahan Diskret bagi Tindak Balas Imun terhadap Sel Abnormal)

ALEH A. AL-SHAMMARI, A.S. RAMBELY* & N.S. KAMARUDIN

Mathematics Program, Faculty of Science & Technology, Universiti Kebangsaan Malaysia, 43600 UKM Bangi, Selangor, Malaysia

Received: 25 February 2025/Accepted: 19 February 2026

ABSTRACT

This study investigates the complex dynamics and control of a discrete-time fractional-order model describing the immune response to abnormal cells. We establish the local asymptotic stability of the equilibrium points and derive the specific parametric conditions governing the emergence of Neimark-Sacker and flip bifurcations. Numerical simulations not only confirm these bifurcations but also show the subsequent onset of chaos. To mitigate this, we successfully implement and demonstrate the efficacy of three control strategies state feedback, pole placement, and hybrid control in stabilizing the chaotic regimes and suppressing undesirable bifurcations. The numerical results provide strong validation of the theoretical analysis, underscoring the value of these control techniques for managing pathological dynamics in immune system models.

Keywords: Discrete immune system model with fractional-order; flip bifurcation; Hopf bifurcation; N-S bifurcation

ABSTRAK

Penyelidikan ini mengkaji dinamik kompleks dan kawalan model tertib pecahan masa diskret yang menggambarkan tindak balas imun terhadap sel yang tidak normal. Kami mewujudkan kestabilan asimptotik tempatan bagi titik keseimbangan dan memperoleh keadaan parametrik khusus yang mengawal kemunculan bifurkasi Neimark-Sacker dan flip. Simulasi berangka bukan sahaja mengesahkan bifurkasi ini tetapi juga mendedahkan permulaan huru-hara berikutnya. Untuk mengurangkan ini, kami berjaya melaksana dan menunjukkan keberkesanan tiga strategi kawalan maklum balas keadaan, penempatan kutub dan kawalan hibrid dalam menstabilkan rejim huru-hara dan menyekat bifurkasi yang tidak diingini. Keputusan berangka memberikan pengesahan yang kukuh terhadap analisis teori, menggariskan nilai teknik kawalan ini untuk mengurus dinamik patologi dalam model sistem imun.

Kata kunci: Bifurkasi flip; bifurkasi Hopf; bifurkasi N-S; model sistem imun diskret dengan tertib pecahan

INTRODUCTION

The immune system is a complex biological network tasked with identifying and eliminating pathogens and abnormal cells, such as cancer cells. Understanding the dynamic interactions between immune components and their targets is crucial for developing therapeutic strategies. While clinical and field studies provide essential data, mathematical modeling offers a complementary tool to uncover underlying dynamics that are difficult to observe empirically. By simplifying reality to its core features, mathematical models can reveal complex behaviors such as bifurcations and chaos, providing insights into system stability and control (Elsadany & Matouk 2015).

Bifurcation theory, pioneered by Poincaré (1885) and later advanced by Hopf, Andronov, and others (Elsadany & Matouk 2015), is fundamental for analyzing such nonlinear dynamics. It allows researchers to predict qualitative changes in a system's behavior as parameters vary. This theory has been extensively applied to biological systems, including models of interacting species that incorporate factors like crowding, time lags, and functional responses (Kesh, Sarkar & Roy 2000; Kundu & Maitra 2018; Song & Xiang 2006).

A significant modern challenge to human health is the rise of noncommunicable diseases (NCDs). The World Health Organization reported that in 2016, NCDs like cardiovascular disease, cancer, chronic respiratory disease, and diabetes were responsible for 71% of global deaths. Notably, internal factors like genetics account for only 5-10% of cancers, while 90-95% are linked to lifestyle and environmental factors (Anand et al. 2019). Modern dietary shifts towards high-calorie, processed foods, low in essential nutrients that can weaken the immune system, increasing susceptibility to diseases like cancer. This underscores the critical role of immune response in preventing and controlling abnormal cell growth.

Since the 1990s, mathematical models have been developed to decipher the dynamics of tumor-immune interactions. These models, often formulated using differential equations, help in understanding the conditions for tumor elimination, persistence, or coexistence. More recent models have even linked factors like obesity to cancer risk and treatment outcomes (Kuznetsov et al. 1994). As Thomas Adams noted in 1618 (Webb, Bain & Page 2017), prevention is better than healing, and these models are vital for promoting preventive health strategies.

A significant advancement in this field is the incorporation of fractional calculus. Fractional-order models provide a more accurate framework for biological systems than classical integer-order models because they inherently capture memory and hereditary properties (Elsadany & Matouk 2015). This makes them exceptionally well-suited for modeling the immune system, whose responses are influenced by past encounters.

While continuous fractional-order models have been studied, the dynamics of their discrete-time counterparts are less explored, presenting a significant gap in the literature. This paper addresses this gap by investigating a discrete-time fractional-order model of the immune response to inhibit and elimination abnormal cells. We build upon the continuous immune-healthy diet model (IHDM) proposed by Alharbi and Rambely (2019), which describes the interaction between immune cells (L) and abnormal cells (M),

$$\frac{dL(t)}{dt} = rL(1-\beta L) - \eta LM, \frac{dM(t)}{dt} = \sigma - \delta M - \frac{\rho LM}{\omega + L} - \mu LM, \quad (1)$$

where $L(0) = L_0 \geq 0$, $M(0) = M_0 \geq 0$. Here the meaning of other parameters is given in Table (1).

The number of parameters in system (1) can be minimized by applying the following transformations:

$$L = \frac{\rho x}{\beta r}, M = \frac{\rho y}{\eta}, t = \frac{\tau}{\rho}.$$

This leads to the following system expressed in dimensionless form:

$$\frac{dx}{d\tau} = x(a - x - y), \frac{dy}{d\tau} = b - cy - \frac{xy}{d+x} - exy \quad (2)$$

where

$$a = \frac{r}{\rho}, b = \frac{\eta\sigma}{\rho^2}, c = \frac{\delta y}{\rho}, d = \frac{\beta r\omega}{\rho}, e = \frac{\mu}{\beta r}.$$

The primary contribution of this work is the analysis of the discrete-time version of this model. We introduce a fractional order α into the system (2) using the Caputo derivative, resulting in:

$$D_\tau^\alpha x(\tau) = x(a - x - y), D_\tau^\alpha y(\tau) = b - cy - \frac{xy}{d+x} - exy. \quad (3)$$

Here, D^a represents the Caputo fractional derivative. Following the discretization method in (El-Sayed & Salman 2013), we derive the discrete-time fractional-order model:

$$x_{n+1} = x_n + \frac{h^\alpha}{\Gamma(\alpha+1)}[x_n(a - x_n - y_n)], y_{n+1} = y_n + \frac{h^\alpha}{\Gamma(\alpha+1)}\left[b - cy_n - \frac{x_n y_n}{d+x_n} - ex_n y_n\right], \quad (4)$$

where $h > 0$ is the step size. The objectives and significance of this study are threefold: To perform a rigorous nonlinear analysis of the discrete map (4), establishing conditions for stability and the existence of bifurcations (flip and Neimark-Sacker), to identify and control chaotic behavior using advanced strategies like state feedback and hybrid control and to provide numerical simulations that validate our theoretical findings, thereby offering deeper insights into the complex dynamics of the immune response. Our results not only enhance the theoretical understanding of discrete fractional systems but also suggest potential frameworks for controlling pathological states, equationing with the broader goal of leveraging mathematical models for preventive healthcare.

TABLE 1. Parameters of model (1)

Parameter	Representation
r	The rate of growth of normal cells
β	Rate of appearance of abnormal cells during the cell life cycle of the normal cell
η	Rate of decrease in the number of immune cells as a result of their interaction with abnormal cells
σ	The fixed source of immune cells
δ	Rate of natural death of immune cells
ρ	The rate of immune system response to resisting abnormal cells
ω	The threshold rate of the immune system
μ	The ability of the immune cells to eliminate abnormal cells or inhibit them

EXISTENCE AND UNIQUENESS

The following theorem provides the sufficient conditions for ensuring the existence and uniqueness of the solution to system (4).

Theorem 1 The existence and uniqueness of the solution for system (4) in the region $\Psi \times (0, T]$, under the initial conditions $X(0) = X_0$ and $t \in (0, T]$, are guaranteed by the following sufficient condition:

$$\Theta = \frac{T^{\alpha}}{\Gamma(1+\alpha)} max\left\{a + \theta\left(3 + e + \frac{d}{(d+\theta)^2}\right), c + \theta\left(1 + e + \frac{1}{d+\theta}\right)\right\}$$

for some $\theta \in R^{+}$.

Proof The immune system's fractional-order response to suppressing and eliminating abnormal cells, as described in model (3), can be expressed in the following manner:

$$D_t^{\alpha} X(t) = F(X(t)), \quad t \in (0,T], \quad X(0) = X_0, \tag{5}$$

where

$$X = [x\ y\ ], X_0 = [x_0\ y_0\ ], F(X) = \left[x(a - x - y)\ b - cy - \frac{xy}{d+x} - exy\right].$$

We know that, the supremum norm of matrix is

$$\|P\| = sup_{t\in(0,T]}|P(t)|,$$

and the norm of matrix $G = \left[g_{ij}[t]\right]$ is

$$\|G\| = \max_{i} \sum_{j} \quad g_{ij}[t].$$

We investigate the conditions under which a solution exists and is unique within the specified region $\psi \times (0, T]$ where

$$\Psi = \{(x,y): max(|x|, |y|) \le \theta\}. \tag{6}$$

Hence, the solution of system (5) is given as follows

$$X = X_0 + \frac{1}{\Gamma(\alpha)} \int_0^t (t-\tau)^{\alpha-1} F(X(\tau)) d\tau = Q(X).$$

Then

$$Q(X_1) - Q(X_2) = \frac{1}{\Gamma(\alpha)} \int_0^t (t-\tau)^{\alpha-1}\left[F(X_1(\tau)) - F(X_2(\tau))\right] d\tau. \tag{7}$$

Thus, we get the following inequality

$$|Q(X_1) - Q(X_2)| \le \frac{1}{\Gamma(\alpha)} \int_0^t (t-\tau)^{\alpha-1}\left[F(X_1(\tau)) - F(X_2(\tau))\right] d\tau.$$

$$\le \frac{1}{\Gamma(\alpha)} \int_0^t (t-\tau)^{\alpha-1}\left[F(X_1(\tau)) - F(X_2(\tau))\right] d\tau. \tag{8}$$

then

$$\|Q(X_1) - Q(X_2)\| \le \frac{T^{\alpha}}{\Gamma(1+\alpha)} max\left\{a + \theta\left(3 + e + \frac{d}{(d+\theta)^2}\right), c + \theta\left(1 + e + \frac{1}{d+\theta}\right)\right\} \|X_1 - X_2\|,$$
$$\le \Theta \|X_1 - X_2\|,$$

where

$$\Theta = \frac{T^{\alpha}}{\Gamma(1+\alpha)} max\left\{a + \theta\left(3 + e + \frac{d}{(d+\theta)^2}\right), c + \theta\left(1 + e + \frac{1}{d+\theta}\right)\right\}.$$

If $\Theta < 1$, then, the function $X = Q(X)$ is a contraction mapping, it is concluded that Theorem 1 is proved. □

Next, we will analyze the stability properties of system (4).

DYNAMICAL BEHAVIORS OF THE FRACTIONAL-ORDER DISCRETE IMMUNE SYSTEM MODEL DESIGNED TO CONTROL AND REMOVE ABNORMAL CELLS

STABILITY OF THE FIXED POINTS

In this section, we analyze the asymptotic stability of the fixed points in system (4), which shares the same fixed points as system (3). To begin, the following lemma is required.

Lemma 1

(i) The equilibrium point $\underline{x}$ is classified as a stable node when $|\lambda_i| < 1$, for all $i = 1,2$.
(ii) The equilibrium point $\underline{x}$ is termed a saddle point if one eigenvalue satisfies $|\lambda_i| > 1$, while the other satisfies $|\lambda_i| < 1$.
(iii) The equilibrium point $\underline{x}$ is considered an unstable node if $|\lambda_i| > 1$ for all $i = 1,2$.
(iv) The equilibrium point $\underline{x}$ is referred to as hyperbolic if one eigenvalue satisfies $|\lambda_i| = 1$.

To evaluate the equilibrium points of (4) let

$$x_{n+1} = x_n, y_{n+1} = y_n.$$

The first immune-free equilibrium point is given by $E_0 = (0, \frac{b}{c})$, which always exists. The Jacobian matrix $J(E_0)$ for system (4), evaluated at E_0, is as follows:

$$J(E_0) = \begin{pmatrix} 1 + H(a - \frac{b}{c}) & 0 \\ -\frac{bH}{c}(e + \frac{1}{d}) & 1 - cH \end{pmatrix},$$

where $H = \frac{h^{\alpha}}{\Gamma(\alpha+1)}$.

Theorem 2 The equilibrium point E_0 exhibits at least four distinct topological configurations across all possible parameter values.

(i) E_0 is a stable node if $a < \frac{b}{c}$,
(ii) E_0 is a saddle point if $a > \frac{b}{c}$,
(iii) E_0 is a hyperbolic if $a = \frac{b}{c}$.

Proof The eigenvalues associated with the equilibrium E_0 are $\lambda_{01} = 1 + H(a - \frac{b}{c})$ and $\lambda_{02} = 1 - cH$. Consequently, the equilibrium point of system (4) is hyperbolic. □

Before we study the coexistence point and its stability are studied, the following theorem which is proved in Shoira and Riskeldi (2023).

Theorem 3 (Shoira & Riskeldi 2023)
For the cubic equation $f(x) = px^3 + qx^2 + rx + s = 0$ ($p > 0$ and $s < 0$) has at least one of the following cases

(i) one positive real root $\Leftrightarrow \Delta < 0$,

(ii) three distinct real roots, with one or all of them being positive $\Leftrightarrow q^2 - 3pr > 0$ and $\Delta < 0$,
(iii) one positive real root and two identical roots $\Leftrightarrow q^2 - 3pr > 0$ and $\Delta = 0$,

$$\Delta = f(x_{min})f(x_{max}) = 18pqrs - 27p^2s^2 - 4q^3s - 4pr^3 - q^2r^2 \; x_{max}, x_{min} = \frac{-q \pm \sqrt{q^2 - 4pr}}{3p}.$$

It is noted that, the second equilibrium point is $E_* = (x_*, y_*) = (a - y_*, y_*)$, where y_* represents the root of the polynomial

$$ey_*^3 + q_1y_*^2 + r_1y_* + s_1 = 0$$

where

$$q1 = -(2ae + de + c + 1),\ r_1 = (a^2e + ade + ac + cd + a + b),\ s_1 = -b(a + d),\ \Delta_1 = 18eq_1r_1s_1 - 27e^2s_1^2 - 4q_1^3s_1 - 4er_1^3 - q_1^2r_1^2$$

Then, if $y_* < a$ one of the following cases is true,

(i) a single coexistence equilibrium point $\Leftrightarrow \Delta_1 > 0$,
(ii) three distinct coexistence equilibrium points or one of it $\Leftrightarrow q_1^2 - 3er_1 > 0$ and $\Leftrightarrow \Delta_1 < 0$,
(iii) either one coexistence equilibrium point or two coexistence equilibrium points $\Leftrightarrow q^2 - 3pr > 0$ and $\Delta_1 = 0$.

The Jacobian matrix $J(E_*)$ for system (4), calculated at the equilibrium point E_*, is given by:

$$J(E_*) = \begin{pmatrix} 1 - x_*H & -x_*H & -y_*H\left[\frac{d}{(d+x_*)^2} + e\right] \\ 1 - H(c + \frac{x_*}{d+x_*} + ex_*) & & \end{pmatrix}. \quad (9)$$

The characteristic equation corresponding to the Jacobian matrix $J(E_*)$ is:

$$\lambda^2 - Tr_*\lambda + Det_* = 0, \quad (10)$$

where

$$Tr_* = 2 - (x_* + k_2)H,\ Det_* = 1 - (x_* + k_2)H + x_*(k_2 - k_1)H^2,$$
$$k_1 = y_*\left[\frac{d}{(d+x_*)^2} + e\right],\ k_2 = c + ex_* + \frac{x_*}{d+x_*}.$$

This leads us to the following theorem.

Theorem 4 The equilibrium point E_* exhibits at least four distinct topological configurations across all parameter values:

(i) E_* is asymptotically stable (a sink) if $0 < h < h_1$,
(ii) E_* is unstable (source) if $h > h_2$,
(iii) E_* is a saddle node if $h_1 < h < h_2$,(iv) E_* becomes non-hyperbolic when $h = h_1$ or h_2,

where

$$h_1 = \sqrt[\alpha]{\frac{4\Gamma(1+\alpha)}{k_2 + x_* + \sqrt{\Delta_2}}},\quad h_2 = \sqrt[\alpha]{\frac{4\Gamma(1+\alpha)}{k_2 + x_* - \sqrt{\Delta_2}}},\quad \Delta_2 = (k_2 - x_*)^2 + 4k_1x_* > 0.$$

Proof The eigenvalues associated with the equilibrium point E_* are determined by the roots of the characteristic Equation (10), given by:

$$\lambda_{11}, \lambda_{12} = 1 - \frac{H}{2}\left[k_2 + x_* \pm \sqrt{\Delta_2}\right].$$

Therefore, by applying the stability conditions outlined in Lemma 1, the results *(i)-(iv)*, can be derived. □

BIFURCATIONS

In this section, the conditions under which flip bifurcation and Neimark-Sacker bifurcation occur at the positive fixed point E_* were established.

FLIP BIFURCATION ANALYSIS

The characteristic equation of the Jacobian matrix for system (4), evaluated at the unique fixed point $E_*(x_*, y_*)$, is expressed as:

$$P_*(\lambda) = \lambda^2 - Tr_*\lambda + Det_* = 0 \quad (11)$$

where

$$Tr_* = 2 - (x_* + k_2)H,\ Det_* = 1 - (x_* + k_2)H + x_*(k_2 - k_1)H^2.$$

Equation (11) gives one eigenvalue $\lambda_1 = -1$ and other eigenvalue $\lambda_2 \neq \pm 1$ if and only if $P_*(-1)$, $Tr_* \neq 0, -2$, i.e. $Tr_* + Det_* = -1$. It follows that

$$a = \frac{4 + y_*(k_1 - k_2)H^2 - 2(k_2 - y_*)H}{H(2 + (k_1 - k_2)H)} = a_*(say).$$

Now, let $FB = \{(a, b, c, d, e, a, h): a = a_*, x_* < a\}$. Let a is chosen as bifurcation parameter and let $u_n = x_n - x_*$, $v_n = y - y_*$ and $r = a - a_*$, where r is a sufficiently small variable. By shifting the fixed point $E_*(x_*, y_*)$ of map (4) to the origin, the following is obtained:

$$\begin{pmatrix} u_n \\ v_n \\ r \end{pmatrix} \to \begin{pmatrix} \phi_{11} & \phi_{12} & \phi_{13} & \phi_{21} & \phi_{22} & 0 & 0 & 0 & 1 \end{pmatrix} \begin{pmatrix} u_n \\ v_n \\ r \end{pmatrix} + \begin{pmatrix} f_1(u_n, v_n, r) \\ f_2(u_n, v_n, r) \\ 0 \end{pmatrix}, \quad (12)$$

where

$$f_1(u_n, v_n, r) = \phi_{14}u_n^2 + \phi_{15}u_nv_n + \phi_{16}ru_n + \phi_{17}ru_n^2 + \phi_{18}u_n^3 + \phi_{19}u_n^2v_n + O(|u_n, v_n|^4)\ f_2(u_n, v_n, r)$$
$$= \phi_{23}u_n^2 + \phi_{24}u_nv_n + \phi_{25}u_n^3 + \phi_{26}u_n^2v_n + \phi_{18}u_n^3 + \phi_{19}u_n^2v_n + O(|u_n, v_n|^4)$$

and ϕ_{lm} ($l = 1,2$, $m = 1, 2, 3, 4, 5$) are presented in Appendix (8).

Linearizing map (8) at the point (0, 0, 0)yields:

$$J = (\phi_{11}\,\phi_{12}\,\phi_{13}\,\phi_{21}\,\phi_{22}0\;0\;0\;1).$$

On constructing an invertible matrix T

$$T = \left(\phi_{12}\;\phi_{12}\;0\;\;-1-\phi_{11}\;\lambda_2-\phi_{11}\;\frac{\phi_{13}}{\phi_{12}}\;0\;0\;1\right)$$

and

$$(u_n v_n r) = T(XYr). \tag{13}$$

The map (12) yields

$$(XYr) \rightarrow (-\,1\;0\;0\;0\;\lambda_2\;0\;0\;0\;1)\,(XYr) + (F_1(X,\,Y,\,r)\;\;F_2\,(\,X,\,Y,\,r)\;0). \tag{14}$$

Here

$$F_1(X,\,Y,\,r) = K_{11}(rX + rY) + K_{12}XY + K_{13}X^2 + K_{14}\,Y^2 + O(|X,\,Y,|)^3\;F_2\,(X,\,Y,\,r) = K_{21}(rX + rY) + K_{22}XY + K_{23}X^2 + K_{24}\,Y^2 + O(|X,\,Y,|)^3.$$

and K_{ls} (l = 1,2,s = 1,2,3,4) are presented in Appendix (8).

Based on center manifold theory, the stability of (X,Y) = (0,0) in the neighborhood of r = 0 is determined by a one-parameter family of reduced equations constrained to a manifold, as given by:

$$W^c(0,\,0,\,0,) = \{(X,\,Y,\,r) \in R^3\colon\, Y = h(X,\,r),\, h(0,\,0) = 0,\, Dh\,(0,\,0) = 0\}$$

for X and a small value of r. Additionally, consider:

$$h(X,\,r) = h_1 r^2 + h_2 Xr + h_3 X^2 + O(|X,\,r|^3).$$

Then $h(X,\,r)$ must satisfy

$$N(h(X,\,r)) = h(-X + F_1(X,\,h(X,\,r),\,r,\,r) - \lambda_2 h(X,\,r) - F_2(X,\,h(X,\,r),\,r) = 0. \tag{15}$$

From (11) and (15), we get

$$\mathrm{h}_1 = 0,\;\mathrm{h}_2 = \frac{\mathrm{k}_{24}}{\lambda_2 + 1},\;\mathrm{h}_3 = \frac{\mathrm{k}_{21}}{\lambda_2 - 1}.$$

The map is transformed as follows

$$F{:}X \rightarrow -\,X + k_{11}X^2 + k_{14}rX + O(|X,\,Y|^3) \tag{16}$$

We can see that

$$\Omega_1 = \left(\frac{\partial \mathrm{F}}{\partial \mathrm{r}}\frac{\partial^2 \mathrm{F}}{\partial \mathrm{X}^2} + 2\frac{\partial^2 \mathrm{F}}{\partial \mathrm{X}\partial \mathrm{r}}\right)\Big|_{(0,0)} = 2\,(\mathrm{k}_{14} - \mathrm{k}_{11}) \neq 0 \text{ and } \Omega_2 = \left(\frac{1}{2}\left(\frac{\partial^2 \mathrm{F}}{\partial \mathrm{X}^2}\right)^2 + \frac{1}{3}\frac{\partial^3 \mathrm{F}}{\partial \mathrm{X}^3}\right)\Big|_{(0,0)} = 2\mathrm{k}_{11}^2 \neq 0.$$

Thus, a flip bifurcation takes place in equation (4) at the fixed point E_* when $a = a_*$.

Lemma 2 If $\Omega_2 \neq 0$, then system (4) experiences a flip bifurcation at the unique positive fixed point E_* when the parameter a varies within a small neighborhood of a_*. Furthermore, if $\Omega_2 > 0$ ($\Omega_2 < 0$) the period-two orbit that emerges from the fixed point is stable (unstable). Consequently, the presence of a flip bifurcation indicates that, under certain conditions, the immune system can coexist in a two-period orbit (Figure 1).

The emergence of a flip bifurcation, leading to quasi-periodic oscillations, can be interpreted as a transition in the dynamical behaviour of the immune-abnormal cell interaction prior to bifurcation, the system exhibits stable periodic orbit representing w-existence state, where immune effector cells effectively regulate the abnormal cell population within a controllable within range. As the system parameter a varies, a flip bifurcation occurs, leading to the loss of stability of primany periodic orbit and the appearance of a new oscillation with duble the period. This transition reflects the onset of cyclic immune responsec, characterize by alternating phases of immune dominance and abnormal cell resurgence with further variation of parametens, the system may evolve in to quasi-periodic oscillation, indicating that the immune and abnormal cell population fluctuate in complex yet bounded behavior. Biologically, this quasi-periodic behavior can be interpreted as an adaptive immune regulation process driven by the memory-dependent nature of fractional dynamics, where the immune system continually adjusts its response to maintain dynamic coexistence rather than complete eradication. Such behavior shows the nonlinear and memory-driven resilience of the immune system in sustaining homeostasis under perturbations, and it underscores the potential of fractional-order modeling in capturing the intricate feedbacks underlying immune surveillance and control of abnormal cells.

NEIMARK-SACKER BIFURCATION

A Neimark-Sacker bifurcation at the equilibrium point E_* emerges when the parameters (a, b, c, d, e, a, h) vary within a small vicinity of Ω_3. Additionally, a perturbed version of model (4) can be derived.

$$\begin{aligned} x_{n+1} &= x_n + (H_2 + H_*)x_n(a - x_n - y_n), y_{n+1} \\ &= y_n + (H_2 + H_*)\left[b - cy_n - \frac{x_n y_n}{d + x_n} - ex_n y_n\right], \end{aligned} \tag{17}$$

where $|H_*|$<<1 is a bounded perturbation parameter. Let $U_n = x_n - x_*$, $V_n = y_n - y_*$, and $H = H_2 + H_*$ then we can translate the fixed point E_* to (0, 0), and rewrite (17) as follows:

$$(U_{n+1}\,V_{n+1}) = (c_{11}U_n + c_{12}V_n + c_{13}U_nV_n + c_{14}U_n^2 + c_{15}U_n^2V_n + O(|U_n, V_n|^3)c_{21}U_n + c_{22}V_n + c_{23}U_nV_n + c_{24}V_n^2 + c_{25}U_n^2V_n + O(|U_n, V_n|^3)) \tag{18}$$

where cij(i = 1, 2, j = 1, 2, 3, 4, 5) are presented in Appendix (8).

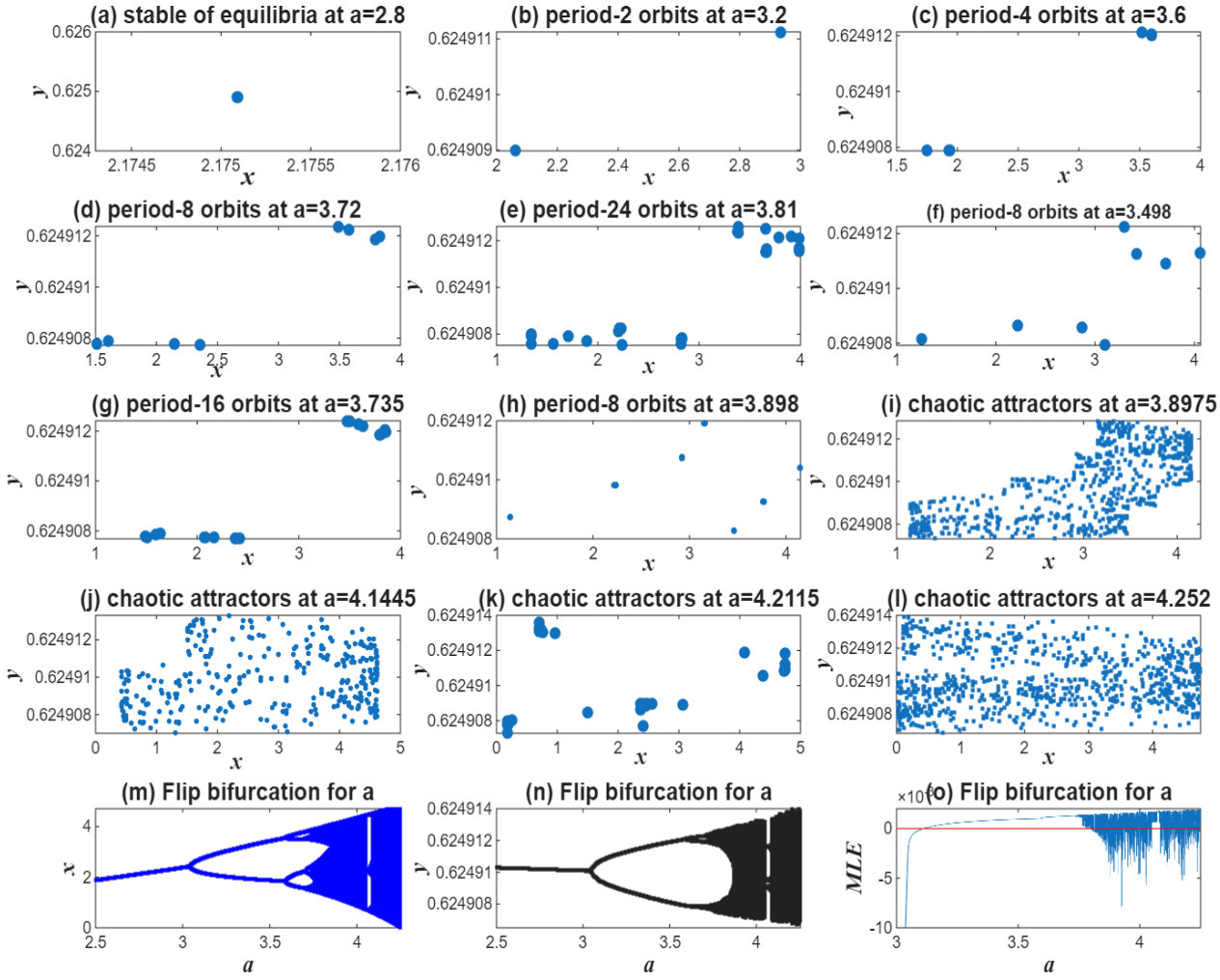

FIGURE 1. Attractor, flip bifurcation diagram and maximal Lyapunov exponent for α

The characteristic equation corresponding to the linearized system of model (18) at the point (0, 0) is:

$$\lambda^2 + f_1(H_*)\lambda + f_2(H_*) = 0, \tag{19}$$

where

$$f_1(H_*) = -(c_{11} + c_{22}) = 2 - G_1(H_2 + H_*),$$
$$f_2(H_*) = c_{11} + c_{22} - c_{21}c_{12} = 1 - G_1(H_2 + H_*) + G_2(H_2 + H_*)^2;$$
$$G_1 = x_* + c + \frac{x_*}{d+x_*} + ex_*$$
$$G_2 = \left((a - 2x_* - y_*)\left(-c - \frac{x_*}{d+x_*} - ex_*\right) + \left(\frac{d}{(d+x_*)^2} + e\right)y_*x_*\right)$$

Since, parameters $(h, a, a, b, c, d) \in \Omega_3$ and H_* lies in a narrow range around $H_* = 0$, the roots of Equation (19) form a complex conjugate pair, labeled λ_1 and λ_2 where,

$$\lambda_{1,2} = \frac{1}{2}\left[-f_1 \pm \sqrt{f_1^2 - 4f_2}\right]$$
$$= -1 + \frac{H+H_*}{2}\left[G_1 \pm i\sqrt{4G_2 - G_1^2}\right]$$

then we have

$$|\lambda_{1,2}| = \sqrt{f_2(H_*)},\ \frac{d|\lambda_{1,2}|}{dH_*}|_{H_*=0} = \frac{G_1}{2} > 0.$$

Moreover, when $H_* = 0$, it is essential that none of the eigenvalues $\underline{\lambda}^n$, $\lambda^n \neq 1$, $(n = 1,2,3,4)$, which is equivalent to requiring that $f_1(0) \neq -2,0,1,2$. Since we have $f_1^2(0) - 4f_2(0) < 0$ and $f_2(0) = 1$, it follows that $f_1^2(0) < 4$; so $f_1(0) \neq \pm 2$. Thus, the only conditions that need to be enforced are $f_1(0) \neq 0, 1$, which implies that

$$G_1^2 \neq 2\underline{G}_2, 3\underline{G}_2. \tag{20}$$

Consequently, the eigenvalues $\lambda_{1,2}$ of the fixed point (0, 0) in Equation (19) do not lie at the intersection of the unit circle with the coordinate axes when $H_* = 0$. Next, we examine the normal form of model (18), when $H_* = 0$. Let $\theta = Re(\lambda_{1,2})$, $\lambda = Im(\lambda_{1,2})$ and

$$T = (c_{12}\ 0\ \theta - c_{11}\ -\eta). \tag{21}$$

Consider the translation herewith

$$(U_n\ V_n) = T\,(u_n\ v_n).$$

Taking T^{-1} on both sides of (18), we get

$$(u_{n+1}\ v_{n+1}) = (\theta - \eta\ \eta\ \theta)\ (u_n\ v_n) + (f_3(u_n + v_n)\ f_4(u_n + v_n)), \tag{22}$$

where

$$f_3(u_n + v_n) = c_{13}[(\theta - c_{11})\ u^2{}_n - \eta u_n v_n],$$
$$f_4(u_n + v_n) = [c_{13}(c_{11} - \theta) + c_{12}\,c_{23}]\left[\tfrac{c_{11}-\theta}{\eta}u_n^2 + u_n v_n\right],$$
$$U_n = c_{12}\,u_n,\ V_n = (\theta - c_{11})\ u_n - \eta v_n.$$

Now, we obtain some partial derivatives of the function f (in Appindex (8)) to substitute them into the following equations.

In accordance with the Hopf bifurcation theory, the discriminatory quantity $\hat{h}$ is defined as:

$$\hat{h} = -Re\left[\tfrac{(1-2\lambda)\bar{\lambda}^2}{1-\lambda}\xi_{11}\xi_{20}\right] - \tfrac{1}{2}|\xi_{11}|^2 - |\xi_{02}|^2 + Re(\bar{\lambda}\xi_{21}) \neq 0, \tag{24}$$

where

$$\lambda = \theta + i\eta,$$
$$\xi_{11} = \tfrac{1}{4}\left[\tfrac{\partial^2 f_3}{\partial u_n^2} + \tfrac{\partial^2 f_3}{\partial v_n^2} + i\left(\tfrac{\partial^2 f_4}{\partial u_n^2} - \tfrac{\partial^2 f_4}{\partial v_n^2}\right)\right]|_{(u_n,v_n)=(0,0)},$$
$$\xi_{20} = \tfrac{1}{8}\left[\tfrac{\partial^2 f_3}{\partial u_n^2} - \tfrac{\partial^2 f_3}{\partial v_n^2} + 2\tfrac{\partial^2 f_4}{\partial u_n \partial v_n} + i\left(\tfrac{\partial^2 f_4}{\partial u_n^2} - \tfrac{\partial^2 f_4}{\partial v_n^2} - 2\tfrac{\partial^2 f_3}{\partial u_n \partial v_n}\right)\right]|_{(u_n,v_n)=(0,0)}, \tag{25}$$
$$\xi_{02} = \tfrac{1}{16}\left[\tfrac{\partial^3 f_3}{\partial u_n^3} + \tfrac{\partial^3 f_3}{\partial u_n \partial v_n^2} + \tfrac{\partial^3 f_4}{\partial u_n^2 \partial v_n} + \tfrac{\partial^3 f_4}{\partial v_n^3} + i\left(\tfrac{\partial^3 f_4}{\partial u_n^3} + \tfrac{\partial^3 f_4}{\partial u_n \partial v_n^2} - \tfrac{\partial^3 f_3}{\partial u_n^2 \partial v_n} - \tfrac{\partial^3 f_3}{\partial v_n^3}\right)\right]|_{(u_n,v_n)=(0,0)}.$$

From this analysis, we have the following theorem.

Theorem 5 Assuming conditions (20) and (25) are satisfied, system (4) experiences a Neimark-Sacker bifurcation at the positive fixed point E_* when the parameter H_* is varied within a small vicinity of H. Furthermore, if ($\hat{h} < 0$, $\hat{h} > 0$), an attracting (or repelling) invariant closed curve bifurcates from E_* for ($H > H_*$, $H < H_*$), respectively.

Bifurcation diagram for h and phase portraits of system (4) are depicted in Figures 2, 3, and 4, respectively.

The onset of chaotic dynamics represents an unpredictable and uncontrolled state of the disease, where small changes in initial conditions (a minor infection) can lead to drastically different outcomes, making treatment prognosis difficult.

CHAOS CONTROL

Managing chaos and bifurcation is vital in population models, particularly those related to the biological reproduction of species. Discrete-time models often display more intricate dynamics than their continuous counterparts. To avoid unpredictable outcomes in populations, it is critical to apply chaos control methods.

POLE PLACEMENT TECHNIQUE

In this subsection, we examine two feedback control strategies aimed at steering unstable trajectories toward stable ones. We begin by applying the OGY method to system (4), a strategy developed by Ott, Grebogi and Yorke (1990). Using the parameter a as a control parameter, we express system (4) as follows:

$$x_{n+1} = x_n + H[x_n(a - x_n - y_n)] = f(x_n, y_n, a), y_{n+1} = y_n + H\left[b - cy_n - \tfrac{x_n y_n}{d+x_n} - ex_n y_n\right] = g(x_n, y_n, a). \tag{26}$$

Here, a is chosen as the control parameter, allowing chaos control to be achieved through minimal perturbations.

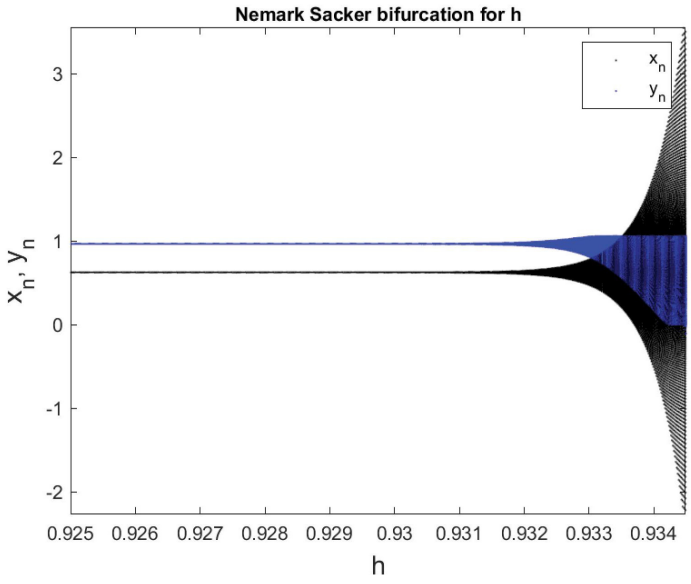

FIGURE 2. Bifurcation diagram for h

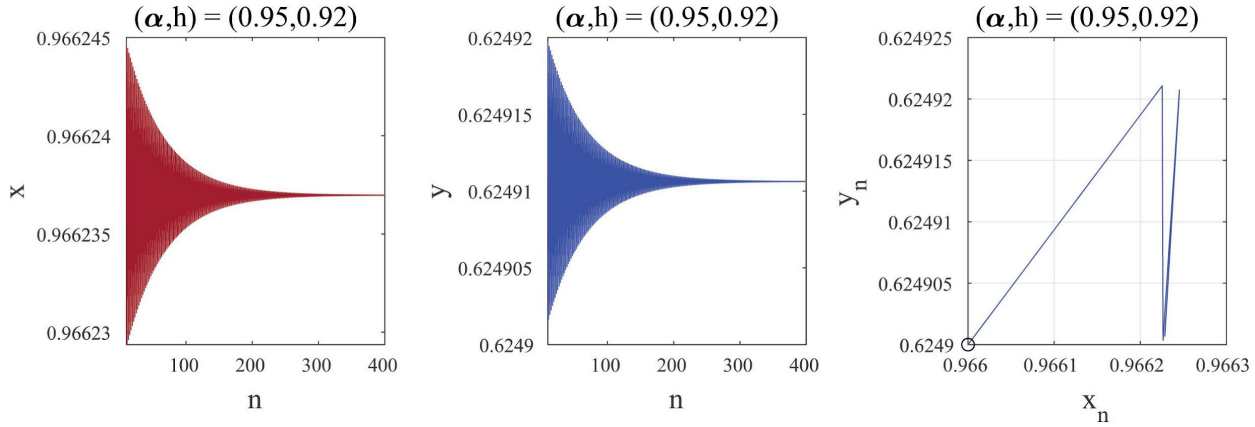

FIGURE 3. Phase portraits of system (4) at (α, *h*) = (0.95, 0.92)

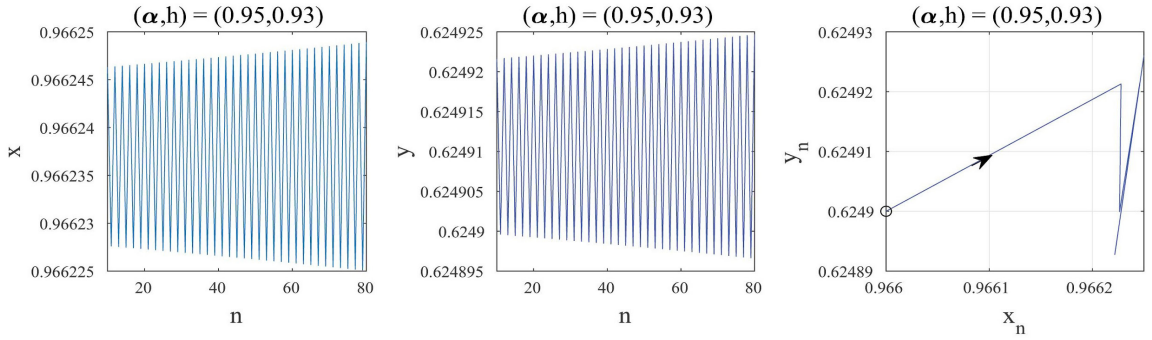

FIGURE 4. Phase portraits of system (4) at (α, *h*) = (0.95, .93)

To implement this, we constrain a to a small interval $\alpha \in (\alpha_0 - \epsilon, \alpha_0 + \epsilon)$, where $\epsilon > 0$ and $a_0$represents the nominal value within the chaotic region. By applying a stabilizing feedback control strategy, the trajectory is guided toward the desired orbit. Let $E_* = (x_*, y_*) = (a - y_*, y_*)$ be an unstable equilibrium point of system (4) in the chaotic region, resulting from period-doubling bifurcation or Neimark-Sacker bifurcation. In the vicinity of this unstable equilibrium point $(a - y_*, y_*)$, system (26) can be approximated by the following linear map:

$$[x_{n+1} - x_* y_{n+1} - y_*] \approx J(x_*, y_*, \alpha_0)[x_n - x_* y_n - y_*] + N[\alpha - \alpha_0]. \quad (27)$$

where

$$J(x_*, y_*, a_0) = [f_x|_{(x_*,y_*,a_0)}\ f_y|_{(x_*,y_*,a_0)}\ g_x|_{(x_*,y_*,a_0)}\ g_y|_{(x_*,y_*,a_0)}]$$
$$= \left[1 - H(a_0 - y_*) \ -H(a_0 - y_*) \ -H\left(\frac{dy_*}{(d + a_0 - y_*)^2} + ey_*\right) 1 \right.$$
$$\left. - H\left(c + \frac{a_0 - y_*}{d + a_0 - y_*} + e(a_0 - y_*)\right)\right]$$

and

$$N = \left[\frac{\partial f(x_*,y_*,a_0)}{\partial a}\ \frac{\partial g(x_*,y_*,a_0)}{\partial a}\right] = [H(a_0 - y_*)\ 0\ ].$$

Additionally, system (26) is controllable if the following matrix condition is satisfied:

$$C = [N{:}JN] = [H(\alpha_0) - y_*)\ H(\alpha - y_*)(1 - H(\alpha_0 - y_*))\ 0 - (\alpha_0 - y_*)H^2 \quad (28)$$

is of rank 2. Moreover, taking $[\alpha - \alpha_0] = -J[x_n - x_* y_n - y_*]$, where $Q = [v_1\ v_2]$, then system (27) can be written as

$$[x_{n+1} - x_* y_{n+1} - y_*] \approx [J - NQ][x_n - x_* y_n - y_*]. \quad (29)$$

Moreover, the controlled version of system (4) is expressed as:

$$x_{n+1} = x_n + H\left[x_n\left((a_0 - v_1(x_n - x_*) - v_2(y_n - y_*)) - x_n - y_n\right)\right], y_{n+1} = y_n + H\left[b - cy_n - \frac{x_n y_n}{d + x_n} - ex_n y_n\right] \quad (30)$$

Moreover, the equilibrium point E_* is considered locally asymptotically stable if and only if eigenvalues of the matrix $[J - NQ]$ are located within the open unit disk. The Jacobian matrix $[J - NQ]$ for the controlled system (30) is expressed as follows:

$$J - NQ = \left[1 - H(a - y_*) - H(a - y_*) - H\left(\frac{dy_*}{(d + a - y_*)^2} + ey_* + v_1\right) 1 - H\left(c + \frac{a - y_*}{d + a - y_*} + e(a - y_*) + v_2\right)\right]$$

The characteristic equation for the Jacobian matrix $[J - NQ]$ is provided by:

$$P_p(\lambda) = \lambda^2 - Tr_p\lambda + Det_p = 0 \tag{31}$$

where

$$Tr_p = \lambda_{p1} + \lambda_{p2} = 2 - q_{p1}H \; Det_p = \lambda_{p1}\lambda_{p2} = 1 - q_{p1}H + q_{p2}H^2 \; q_{p1} = c + \frac{a - y_*}{d + a - y_*} + (e + 1)(a - y_*) + v_2 \; q_{p2} = (a - y_*)\left(c + \frac{a - y_*}{d + a - y_*} + e(a - 2y_*) + v_2 - \frac{y_* d}{(d + a - y_*)^2} - v_1\right). \tag{32}$$

Here, λ_{p1} and λ_{p2} represent the roots of the characteristic (Equation 31).

Next, we take $\lambda_{p1} = \pm 1$ and $\lambda_{p1}\lambda_{p2} = 1$ to determine the lines of marginal stability for the corresponding controlled system, these constraints ensure that λ_{p1} and λ_{p2} lie within the open unit disk. Assuming $\lambda_{p1}\lambda_{p2} = 1$, Equation (32) leads to:

$$L_1(v_1, v_2): q_{p1} = q_{p2}H \tag{33}$$

Moreover, we assume that $\lambda_{p1} = 1$, then (32) yield that:

$$L_2(v_1, v_2): c + \frac{a - y_*}{d + a - y_*} + e(a - 2y_*) + v_2 = \frac{y_* d}{(d + a - y_*)^2} + v_1 \tag{34}$$

Finally taking $\lambda_{p1} = -1$, then, from Equations (32) we get

$$L_3(v_1, v_2): q_{p2}H^2 - 2q_{p1}H + 4 = 0. \tag{35}$$

First, stable eigenvalues are located within a triangular region in the v_1v_2-plane, which is enclosed by the lines L_1, L_2, *and* L_3 for specific parameter values. To manage the chaos caused by bifurcation in (4), we employ a hybrid control feedback method as described by Luo et al. (2003). This method was initially designed to manage period-doubling bifurcations, (Figures 6 & 7).

Figure (5) shows the stability region for the controlled system (30) bounded by lines L_1, L_2, *and* L_3.

HYBRID CONTROL METHOD

Additionally, Yuan and Yang (2015) utilized the same technique to control chaos resulting from Neimark-Sacker bifurcations. If system (4) experiences bifurcation at E_*, the associated controlled system is represented as:

$$x_{n+1} = v(x_n + H[x_n(a - x_n - y_n)]) + (1 - v)x_n, y_{n+1} = v\left(y_n + H\left[b - cy_n - \frac{x_n y_n}{d + x_n} - ex_n y_n\right]\right) + (1 - v)y_n. \tag{36}$$

where $0 < v < 1$. The control strategy outlined in (36) integrates both parameter perturbation and feedback control. By carefully choosing the control parameter v, the period-doubling bifurcation and Neimark-Sacker bifurcation at the equilibrium point E_* of the controlled system (36) can be either accelerated, postponed, or completely removed. The Jacobian matrix of the controlled system (36), evaluated at E_*, is expressed as:

$$J_h(E_*) = \left(1 - x_* vH - x_* H - y_* vH\left[\frac{d}{(d + x_*)^2} + e\right] 1 - vH\left(c + \frac{x_*}{d + x_*} + ex_*\right)\right). \tag{37}$$

The characteristic equation corresponding to the Jacobian matrix $J_n(E_*)$ is

$$P_n(\lambda) = \lambda^2 - Tr_n\lambda + Det_n = 0, \tag{38}$$

where

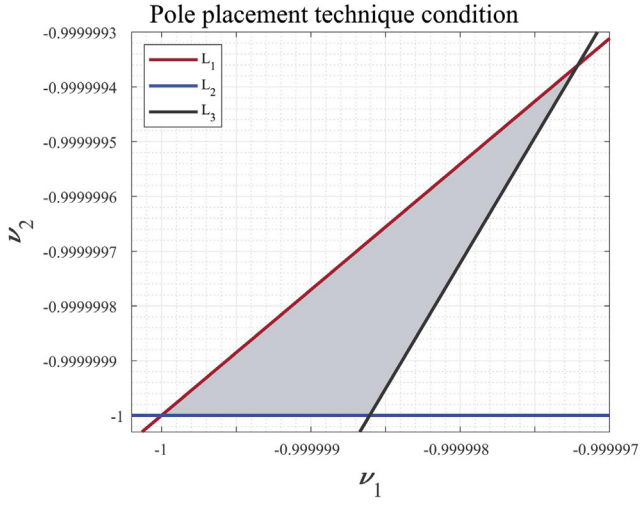

FIGURE 5. The stability region for the controlled system (30)

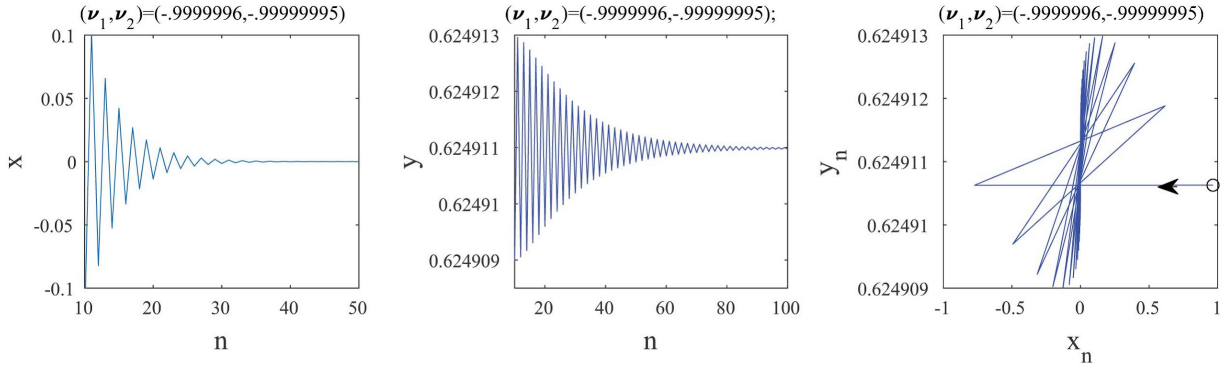

FIGURE 6. Phase portraits of system (30) at $(v_1, v_2) = (-0.9999996, -$ (inside region bounded by L_1, L_2, and L_3)

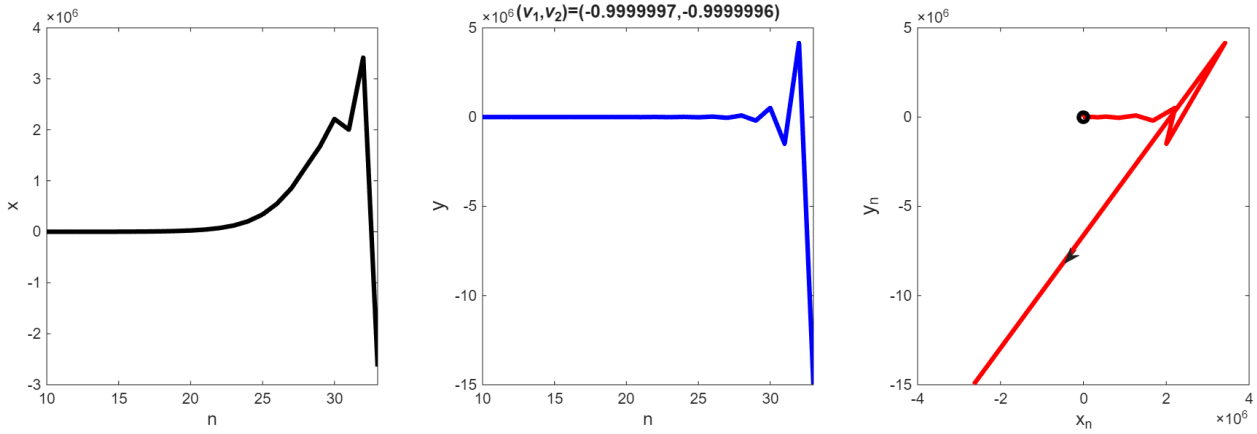

FIGURE 7. Phase portraits of system (30) at $(v_1, v_2) = (-0.9999997, -0.9999996)$ (outside region bounded by L_1, L_2, and L_3)

$$Tr_n = 2 - (x_* + k_2)\, vH,\ Det_n = 1 - (x_* + k_2)vH + x_*(k_2 - k_1)\, v^2 H^2$$

For the stability of the system (36), $P_n(1) > 0$, $P_n(-1) > 0$ and $P_n(0) < 0$, where

$$P_n(1) = (k_2 - k_1)x_*\, v^2 H^2 > 0\ P_n(-1) = 4 + (k_2 - k_1)x_*\, v^2 H^2 - 2(k_2 + x_*)\, vH > 0\ P_n(0) = 1 + (k_2 - k_1)x_*\, v^2 H^2 - (k_2 + x_*)\, vH < 0. \quad (39)$$

The following Lemma establishes the conditions for the local asymptotic stability of E_* in the controlled system (36).

Lemma 5.1 The positive equilibrium E_* of the controlled system (36) is locally asymptotically stable provided the following conditions are satisfied:

$$(k_2 - k_1)v^2 > 04 + (k_2 - k_1)x_*\, v^2 H^2 - 2(k_2 + x_*)vH > 01 + (k_2 - k_1)\, x_*\, v^2 H^2 - (k_2 + x_*)vH < 0 \quad (40)$$

STATE FEEDBACK CONTROL

State feedback control provides an optimal approach to managing chaotic systems (Din 2017). This technique transforms the chaotic system into a piecewise linear system through the use of an optimal controller. It reduces the upper bound and, under specific conditions, enables control within the system. By applying an appropriate control mechanism, the resulting controlled system derived from (4) is expressed as:

$$x_{n+1} = x_n + H[x_n(a - x_n - y_n)] + j_1(x_n - x_*), y_{n+1} = y_n + H\left[b - cy_n - \frac{x_n y_n}{d + x_n} - ex_n y_n\right] + j_2(y_n - y_*). \quad (41)$$

represents the desired control force under the feedback control law, where j_1 and j_2 are the feedback gains. The Jacobian matrix of system (41) yields the following characteristic equation:

$$P_s(\lambda) = \lambda^2 - (2 + j_1 + j_2 - (k_2 + x_*)\, H)\lambda + (k_2 - k_1)\, x_* H^2 - (j_1\, k_2 + j_2 x_* + k_2 + x_*)\, H + j_1 j_2 + j_1 + j_2 + 1 = 0 \quad (42)$$

Let λf_1 and λf_2 be two solutions of the characteristic Equation (42) then

$$\begin{aligned}\lambda f_1 + \lambda f_2 = 2 + j_1 + j_2 - (k_2 + x_*)H \; \lambda f_1 \lambda f_2 = (k_2 - k_1) \\ x_* H^2 - (j_1 k_2 + j_2 x_* + k_2 + x_*)\, H + j_1 j_2 + j_1 + j_2 + 1\end{aligned} \tag{43}$$

The conditions defining the marginal stability lines are now provided as follows:

$$\lambda f_1 = \pm 1, \; \lambda f_1 \lambda f_2 = 1$$

then, for the second condition, Equation (42) provides:

$$\begin{aligned}FC_1\text{: } (k_2 - k_1)x_* H^2 - (j_1 k_2 + j_2 x_* + k_2 + x_*)H + \\ j_1 j_2 + j_1 + j_2 = 0.\end{aligned} \tag{44}$$

For another condition of stability, if $\lambda f_1 = 1$ we get

$$FC_2\text{: } (k_1 - k_2)x_* H^2 + (j_1 k_2 + j_2 x_*)H - j_1 j_2 = 0. \tag{45}$$

Similarly for $\lambda f_1 = -1$, it is obtained

$$\begin{aligned}FC_3\text{: } (k_2 - k_1)x_* H^2 - (j_1 k_2 + j_2 x_* + 2k_2 - 2x_*)H + \\ j_1 j_2 + 2j_1 + 2j_2 + 4 = 0.\end{aligned} \tag{46}$$

For stability, all eigenvalues must lie within the triangular region defined by the lines FC_1, FC_2, and FC_3. Thus, it can be inferred that system (41) is stable if its corresponding eigenvalues fall within the open unit disk.

The successful application of pole placement technique, the hybrid control method and state feedback control demonstrates a theoretical intervention strategy. In a clinical context, this could be analogous to an immunotherapy that adjusts the immune system's response parameters to steer it back to a stable, healthy state.

NUMERICAL SIMULATION

In this section, numerical behaviors of model (4) is explored using the analytical framework established in earlier sections. Since most fractional-order differential equations do not have exact analytical solutions, approximation methods and numerical techniques are essential for their study. In all our figures, we take the same parameters as in Alharbi and Rambely (2019) i.e., $r = 0.431201$, $\beta = 2.99 \times 10^6$, $\sigma = 0.7$, $\delta = 0.57$, $m = 0.3389$; $\rho = 0.2710$; $\eta = 0.1379$, $\mu = 0.8130$, which implies that $b = 1.3144$, $c = 2.1033$, $d = 1.6123 \times 10^6$, $e = 6.3 \times 10^{-7}$ and we well take $a = 0.95$, $(x_1, y_1) = (0.966, 0.6249)$ in all figures and other parameter in the neighborhood of the values in Table 1.

Figure (1(a)) illustrates the stable equilibrium of model (4) based on the specified parameter values. An attracting invariant emerges as the fractional-order parameter increases within the range a ϵ (2.8, 4.252). Period-2, 4, 8, 16, and 24 orbits are depicted in Figure (1(b)) to (1(h)). From Figure (1(m)) to (1(o)), the flip bifurcation diagram and maximal Lyapunov exponent are shown for a, with the numerical simulation results confirming our theoretical analysis.

A stable fixed point at a low level of abnormal cells (M) corresponds to a healthy state where the immune system successfully suppresses the tumor (at $a = 2.8$), leading to long-term dormancy or elimination.

The occurrence of a Neimark-Sacker (N-S) bifurcation is demonstrated in Figure 2. This figure shows that the equilibrium point E_* remains stable for $h < 0.925$ but loses stability through an N-S bifurcation at $h < 0.925$. Phase portraits for various values of h, corresponding to Figure 2, are displayed in Figures 2 and 3 to further illustrate these findings.

To control chaos in system (26), the state feedback method is applied. For the conditions (33)-(35) defining the lines of marginal stability, the controllability of system (26) is achieved by introducing a feedback force with $(v_1, v_2) = (-0.9999996, -0.99999995)$ where v_1 and v_2 are selected from the triangular region bounded by the marginal lines L_1, L_2, and L_3 (Figure 5). A stable time series, shown in Figure 4, confirms that system (26) exhibits stable behavior under these parameter settings.

Conversely, if $(v_1, v_2) = (-0.9999997, -0.99999996)$ are chosen outside the triangular region bounded by the marginal lines L_1, L_2, and L_3 (Figure 5), an unstable time series, depicted in Figure (5), indicates that system (26) displays unstable behavior under these conditions.

TABLE 2. Parameters of figures

	α	h
Figure 1	2.5: 4. 255	0.8
Figures 2, 3	1.5911	0.95, 0.92
Figure 4	1.5911	0.93
Figures 5, 6, 7	1.5911	0.8

CONCLUSIONS

This study has presented a comprehensive nonlinear analysis of a discrete-time fractional-order model representing the immune system's response to abnormal cells. We have rigorously established the conditions for the local asymptotic stability of the equilibrium points and derived the specific parametric criteria governing the emergence of Neimark-Sacker and flip bifurcations. Numerical simulations not only confirmed these theoretical findings but also showed a rich spectrum of dynamical behaviors, including period-doubling cascades and chaotic attractors, the latter being quantified using the Maximum Lyapunov Exponent (MLE).

The excellent agreement between our analytical results and numerical simulations validates the theoretical framework and underscores the model's utility in capturing the complex, often chaotic, dynamics inherent in immune-tumor interactions. Furthermore, we successfully demonstrated that chaos control strategies namely, state feedback, pole placement, and hybrid controlare effective in stabilizing the system and suppressing pathological bifurcations. This provides a crucial mathematical foundation for potential intervention strategies.

While this study offers significant insights, it also opens several avenues for future work. The current model, while insightful, could be enhanced by incorporating time delays to represent the maturation time of immune cells or the delayed effects of immune signaling. Expanding the model to include a more detailed sub-population of immune cells (e.g., Cytotoxic T-cells, Natural Killer cells, and T-regulatory cells) to capture a more realistic immune network. Validating the model predictions against experimental or clinical data to refine parameter estimates and improve its biological predictive power. Exploring the application of other advanced control theories, such as adaptive or optimal control, to develop more efficient and robust strategies for stabilizing the immune response.

In conclusion, this work not only deepens the theoretical understanding of discrete fractional-order systems in biology but also provides a versatile framework for analyzing and controlling the complex dynamics of the immune response. The methodologies developed here, as supported by prior research (Din, Naseem & Shabbir 2024), are readily applicable to other high-dimensional discrete systems in mathemamatical biology and beyond.

REFERENCES

Anand, P. et al. 2019

Alharbi, S.A. & Rambely, A.S. 2019. A dynamic simulation of the immune system response to inhibit and eliminate abnormal cells. *Symmetry* 11(4): 572.

Din, Q. 2017. Complexity and chaos control in a discrete-time prey-predator model. *Communications in Nonlinear Science and Numerical Simulation* 49: 113-134.

Din, Q., Jameel, K. & Shabbir, M.S. 2024. Discrete-time predator–prey system incorporating fear effect: Stability, bifurcation, and chaos control. *Qualitative Theory of Dynamical Systems* 23(Suppl 1): 285.

Elsadany, A. & Matouk, A. 2015. Dynamical behaviors of fractional-order Lotka–Volterra predator–prey model and its discretization. *Journal of Applied Mathematics and Computing* 49: 269-283.

El-Sayed, A. & Salman, S. 2013. On a discretization process of fractional-order Riccati differential equation. *J. Fract. Calc. Appl.* 4(2): 251-259.

Kesh, D., Sarkar, A. & Roy, A. 2000. Persistence of two prey–one predator system with ratio-dependent predator influence. *Mathematical Methods in the Applied Sciences* 23(4): 347-356.

Kundu, S. & Maitra, S. 2018. Qualitative analysis of a three species predator–prey model with stochastic fluctuation. *Applications of Fluid Dynamics: Proceedings of ICAFD* 2016. Springer. pp. 643-659.

Kuznetsov, V.A., Makalkin, I.A., Taylor, M.A. & Perelson, A.S. 1994. Nonlinear dynamics of immunogenic tumors: Parameter estimation and global bifurcation analysis. *Bulletin of Mathematical Biology* 56(2): 295-321.

Luo, X.S., Chen, G., Wang, B.H. & Fang, J.Q. 2003. Hybrid control of period-doubling bifurcation and chaos in discrete nonlinear dynamical systems. *Chaos, Solitons & Fractals* 18(4): 775-783.

Ott, E., Grebogi, C. & Yorke, J.A. 1990. Controlling chaos. *Physical Review Letters* 64: 1196.. Erratum: Controlling chaos. *Physical Review Letters* 64: 2837.

Poincaré, H. 1885. Sur l'équilibre d'une masse fluide animée d'un mouvement de rotation. *Bulletin astronomique, Observatoire de Paris* 2(1): 109-118.

Shoira, A. & Riskeldi, T. 2023. Theorems on the number of roots of a cubic equation and their location as a means of developing students'visual thinking. *Physical and Mathematical Education* 38(4): 7-13.

Song, X. & Xiang, Z. 2006. The prey-dependent consumption two-prey one-predator models with stage structure for the predator and impulsive effects. *Journal of Theoretical Biology* 242(3): 683-698.

Vayenas, D.V., Aggelis, G., Tsagou, V. & Pavlou, S. 2005. Dynamics of a two-prey–one-predator system with predator switching regulated by a catabolic repression control-like mode. *Ecological Modelling* 186(3): 345-357.

Webb, P., Bain, C. & Page, A. 2017. *Essential Epidemiology: An Introduction for Students and Health Professionals*. Cambridge: Cambridge University Press.

Yuan, L.G. & Yang, Q.G. 2015. Bifurcation, invariant curve and hybrid control in a discrete-time predator–prey system. *Applied Mathematical Modelling* 39(8): 2345-2362.

* Corresponding author; email: asr@ukm.edu.my

APPENDIX

8.1 Some requirements of Lemma (2)

$$\phi_{11} = 1 + H(rs - 2x_* - y_*), \phi_{12} = -Hx_*, \phi_{13} = Hx_*, \phi_{14} = -H, \phi_{15} = -H, \phi_{16} = H, \phi_{17} = 0, \phi_{18} = 0, \phi_{19} = 0, \phi_{21} = -H\left(\frac{y_* d}{(d+x_*)^2} + ey_*\right),$$
$$\phi_{22} = 1 - H\left(c - \frac{x_*}{d+x_*} + ex_*\right), \phi_{23} = \frac{Hy_* d}{(d+x_*)^3}, \phi_{24} = -H\left(\frac{d}{(d+x_*)^2} + e\right), \phi_{25} = \frac{-Hy_*}{(d+x_*)^3}, \phi_{26} = \frac{Hd}{(d+x_*)^3};$$

$$K_{11} = \frac{\phi_{15}(\lambda_2-\phi_{11})-\phi_{12}\phi_{24}}{1+\lambda_2}\phi_{13} + \frac{\phi_{16}(\lambda_2-\phi_{11})}{1+\lambda_2}, K_{12} = 2\phi_{12}\left(\frac{\phi_{14}(\lambda_2-\phi_{11})-\phi_{12}\phi_{23}}{1+\lambda_2}\right) + \frac{\phi_{15}(\lambda_2-\phi_{11})-\phi_{12}\phi_{24}}{1+\lambda_2}(\lambda_2 - 2\phi_{11} - 1), K_{13} = \phi_{12}\left(\frac{\phi_{14}(\lambda_2-\phi_{11})-\phi_{12}\phi_{23}}{1+\lambda_2}\right) - \frac{\phi_{15}(\lambda_2-\phi_{11})-\phi_{12}\phi_{24}}{1+\lambda_2}(\phi_{11}+1)\, K_{14} = \phi_{12}\left(\frac{\phi_{14}(\lambda_2-\phi_{11})+\phi_{12}\phi_{23}}{1+\lambda_2}\right) + \frac{\phi_{15}(\lambda_2-\phi_{11})-\phi_{12}\phi_{24}}{1+\lambda_2}(\lambda_2 - \phi_{11})$$

$$K_{21} = \frac{\phi_{15}(1+\phi_{11})+\phi_{12}\phi_{24}}{1+\lambda_2}\phi_{13} + \frac{\phi_{16}(1+\phi_{11})}{1+\lambda_2}\phi_{12}, K_{22} = 2\phi_{12}\frac{\phi_{14}(1+\phi_{11})+\phi_{12}\phi_{23}}{1+\lambda_2} + \left(\frac{\phi_{15}(1+\phi_{11})+\phi_{12}\phi_{24}}{1+\lambda_2}\right)(\lambda_2 - 2\phi_{11} - 1), K_{23} = \phi_{12}\frac{\phi_{14}(1+\phi_{11})+\phi_{12}\phi_{23}}{1+\lambda_2} - \left(\frac{\phi_{15}(1+\phi_{11})+\phi_{12}\phi_{24}}{1+\lambda_2}\right)(\phi_{11}+1), K_{24} = \phi_{12}\frac{\phi_{14}(1+\phi_{11})+\phi_{12}\phi_{23}}{1+\lambda_2} + \left(\frac{\phi_{15}(1+\phi_{11})+\phi_{12}\phi_{24}}{1+\lambda_2}\right)(\lambda_2 - \phi_{11}).$$

8.2 Some requirements of Theorem (5)

$$c_{11} = 1 - c_{13}\left(a - 2x_* - y_*\right), c_{12} = c_{13}x_*, c_{13} = -H_2 - H_*, c_{14} = c_{13}, c_{15} = 0, c_{21} = c_{23}y_*,$$
$$= 1 + c_{13}\left(c + \frac{x_*}{d+x_*} + ex_*\right), c_{23} = c_{13}\left(\frac{d}{(d+x_*)^2} + e\right), c_{24} = 0, c_{25} = \frac{-c_{13}d}{(d+x_*)^3}.$$

$$c_{11} = 1 - c_{13}(a - 2x_* - y_*), c_{12} = c_{13}x_*, c_{13} = -H_2 - H_*, c_{14} = c_{13}, c_{15} = 0, c_{21} = c_{23}y_*, c_{22} = 1 + c_{13}\left(c + \frac{x_*}{d+x_*} + ex_*\right), c_{23} = c_{13}\left(\frac{d}{(d+x_*)^2} + e\right), c_{24} = 0, c_{25} = \frac{-c_{13}d}{(d+x_*)^3}.$$

$$\frac{\partial^2 f_3}{\partial u_n^2} = 2c_{13}\left(\theta - c_{11}\right), \frac{\partial^2 f_3}{\partial u_n \partial v_n} = -\eta c_{13}, \frac{\partial^2 f_3}{\partial v_n^2} = 0, \frac{\partial^3 f_3}{\partial u_n^3} = \frac{\partial^3 f_3}{\partial u_n^2 \partial v_n} = \frac{\partial^3 f_3}{\partial u_n \partial v_n^2} = \frac{\partial^3 f_3}{\partial v_n^3} = 0,$$
$$\frac{\partial^2 f_4}{\partial u_n^2} = \frac{2\left(c_{11}-\theta\right)}{\eta}\left[c_{13}\left(c_{11}-\theta\right) + c_{12}c_{23}\right], \frac{\partial^2 f_4}{\partial u_n \partial v_n} = c_{13}\left(c_{11}-\theta\right) + c_{12}c_{23}, \quad \frac{\partial^2 f_4}{\partial v_n^2} = 0, \quad (23)$$
$$\frac{\partial^3 f_4}{\partial u_n^3} = \frac{\partial^3 f_4}{\partial u_n^2 \partial v_n} = \frac{\partial^3 f_4}{\partial u_n \partial v_n^2} = \frac{\partial^3 f_4}{\partial v_n^3} = 0.$$